Steroid bioconjugation to a CYP3A4 allosteric site and its effect on substrate binding and coupling efficiency

Vanja Polic[a], Irina F. Sevrioukova[b], Karine Auclair*[a]

[a]Department of Chemistry, McGill University, 801 Sherbrooke Street West, Montreal, Quebec, Canada H3A 0B8
[b]Department of Molecular Biology and Biochemistry, University of California, Irvine, California 92697, United States
*Corresponding author: karine.auclair@mcgill.ca

Abstract

Human cytochrome P450 3A4 (CYP3A4) is an important drug metabolizing enzyme involved in a number of drug-drug and food-drug interactions. As such, much effort has been devoted into investigating its mechanism of interaction with ligands. CYP3A4 has one of the highest levels of substrate promiscuity for an enzyme, and can even bind multiple ligands simultaneously. The location and orientation of these ligands depend on the chemical structure and stoichiometry, and are generally poorly understood. In the case of the steroid testosterone, up to three copies of the molecule can associate with the enzyme at once, likely two in the active site and one at a postulated allosteric site. Recently, we demonstrated that steroid bioconjugation at the allosteric site results in an increase in activity of CYP3A4 toward testosterone and 7-benzyloxy-4-trifluoromethylcoumarin oxidation. Here, using the established bioconjugation methodology, we show how steroid bioconjugation at the allosteric site affects the heme spin state, the binding affinity (K_S) of CYP3A4 for testosterone, as well as the enzyme coupling efficiency.

Keywords

Cytochrome P450 3A4; allostery; progesterone; testosterone; coupling; heme spin-state

Introduction

Human cytochrome P450 3A4 (CYP3A4) is responsible for the metabolism of over 50% of existing drugs [1]. It belongs to a large and ubiquitous family of enzymes that is also involved in the biosynthesis of many diverse molecules (*e.g.* vitamins, steroids, secondary metabolites, bile acids) [1]. The clinical importance of CYP3A4 in drug metabolism and its implication in drug-drug interactions [2,3] are major incentives to fully elucidate the ligand-binding mechanism of this enzyme.

Abbreviations: BFC, 7-benzyloxy-4-trifluoromethylcoumarin; CPR, cytochrome P450 reductase; CYP3A4, human cytochrome P450 3A4; DTT, 1,4-dithiothreitol; HFC, 7-hydroxy-4-trifluoromethylcoumarin; NADPH, nicotinamide adenine dinucleotide phosphate reduced; STM, a steroid maleimide derivative; TCEP, tris(2-carboxyethyl)phosphine; TST, testosterone; TST-OH, hydroxytestosterone.

Owing to its large and flexible active site [4–14], CYP3A4 can oxidize substrates varying greatly in size (*e.g.* ranging from xylene at 106 Da, to cyclosporine at 1202 Da) [15,16], and can even bind multiple ligands simultaneously. Global analysis of multiple kinetic parameters suggests that this monomeric enzyme can bind up to three molecules of testosterone (TST), progesterone, α-naphthoflavone or carbamazepine [17–19]. The latter ability could explain the deviations from simple enzyme kinetics observed for some CYP3A4 reactions [5,20–23].

The presence of an allosteric binding site in CYP3A4 has also been suggested [5,20,24–32]. Noteworthy is a crystal structure of CYP3A4 with a co-crystallized steroid molecule, progesterone, at the periphery of the enzyme, suggesting that this region could be an allosteric pocket (Figure 1) [5,25]. The relevance of this X-ray structure is debated because the pocket is at the interface of an unnatural dimer, yet the same area of the protein has been identified by mutagenesis [26–28] and by FRET studies as a potential allosteric site [29]. Although ligand interactions with CYP3A4 remain challenging to study, several ligand binding mechanisms have been proposed. In the case of the steroid TST, it is thought that the first binding event (higher affinity) occurs at the allosteric site, while the two subsequent binding events take place in the active site [17]. The first TST binding event induces some high-spin shift in the heme iron, which may promote the transfer of electrons from the redox partner to CYP3A4 without product formation [17,19]. The subsequent active site binding event results in product formation, whereas association of the third TST molecule improves the enzyme coupling efficiency (ratio of oxidized substrate to the reducing equivalents consumed) [17–19]. A similar mechanism has been proposed for other substrates as well [18,19]. Whether the apparent allosteric behavior of CYP3A4 is a true property of the enzyme or an artifact of a complicated substrate binding mechanism remains debated [33].

We have recently reported the use of steroid bioconjugation to CYP3A4 as a complementary tool to study the postulated allosteric site and explore its effect on enzyme kinetics [34]. *Via* bioconjugation of a steroid-maleimide derivative (STM, Figure 1; previously named PgM) selectively at the allosteric site, we have reported a positive effect on the kinetic activity of CYP3A4 towards two substrates, 7-benzyloxy-4-trifluoromethylcoumarin (BFC) and TST. Here, we build on these results and explore the significance of steroid bioconjugation at the putative allosteric site on substrate affinity and coupling efficiency.
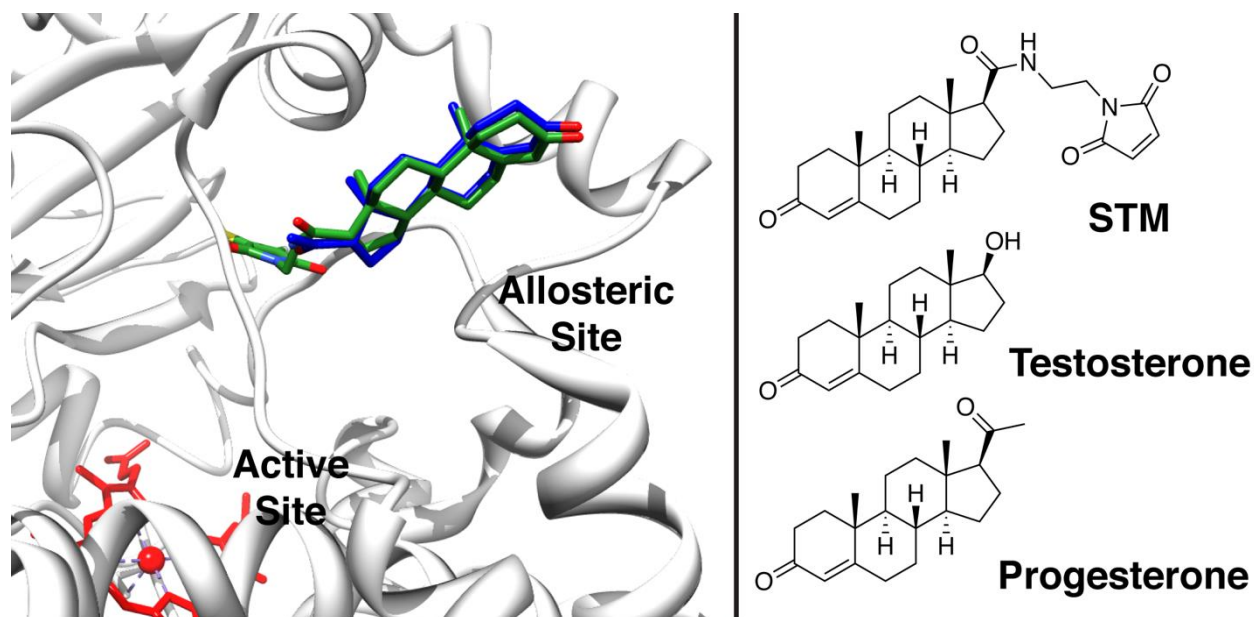
Figure 1. A modified X-ray crystal structure image showing steroid-maleimide (STM) conjugated to C215 of a CYP3A4 mutant. STM (in green) is superimposed on the existing, co-crystallized progesterone (in blue). STM and C215 were built into the allosteric site of CYP3A4 using the USCF Chimera package[35], PDB structure 1W0F[5] and the Persistence of Vision ™ Raytracer. Chemical structures of the steroids and STM are shown for comparison.

Materials and Methods

General Information

All reagents were purchased from Sigma-Aldrich Canada Ltd. (Oakville, ON, Canada), Alfa Aesar (Ward Hill, MA, USA), Chem-Impex (Wood Dale, IL, USA), Agilent Technologies Canada Inc. (Mississauga, ON, Canada) or BioRad (Mississauga, ON, Canada). Reagents were used without further purification. CYP3A4 and CPR plasmids were generously provided by Dr. J. R. Halpert (University of Connecticut) and Dr. C. B. Kasper (University of Wisconsin), respectively.

Expression and purification of wild type and the C215 mutant of CYP3A4

Wild type CYP3A4 and the C215 mutant were expressed and purified as previously described, with minor modifications [34,36]. Wild type refers to the N-terminus-truncated Δ2-12 CYP3A4, which was used as a template for preparation of the C215 mutant containing the following mutations: C58T/C64A/C98S/F215C/C239S/C468G. For protein expression, the cells were harvested at $5000 \times g$ instead of $4000 \times g$. For lysis, 1.3 μg/mL aprotinin and 1.25% 3-[(3-cholamidopropyl)dimethylammonio]-1-propanesulfonate (CHAPS) were supplemented instead of 1 μg/mL aprotinin and 1% CHAPS, while concentrations of other protease inhibitors were kept the same as published. The lysed sample was split into 3 beakers and sonication was performed at 80% cycle duty. Both the Ni-NTA agarose column and Macro-Prep High S Support column were run at a slower flow rate (0.6 mL/min). The protein concentration was calculated

from the reduced CO spectrum only, using a molar extinction coefficient of 91 mM^{-1} cm^{-1} between 450 and 490 nm [37].

Expression and purification of cytochrome P450 reductase (CPR)

CPR was expressed and purified as previously described with minor changes [38]. For CPR expression, the starting culture was generated by inoculating 100 mL of lysogeny broth (LB) with 8 colonies. The overnight culture was then used to inoculate the bulk culture (12 mL in 1 L) for 10 L total volume (10 flasks × 1 L). Following expression, the cells were harvested by centrifugation at 3000 × g and resuspended in 10 mL of 0.1 M potassium phosphate buffer (PBS, pH 7.4) before storage at -80°C. For protein purification, the original protocol was shortened by condensing the two lysis steps into one step, and the two sonication steps into one step. In this case, the PBS buffer was removed by centrifugation at 3000 × g and the pellet was resuspended in 40 mL TSE buffer (75 mM tris buffer, pH 8, with 250 mM sucrose and 250 mM EDTA), after which lysozyme (1.2 mg in 20 mL TSE buffer) was added and the suspension was incubated for 20 min at 4°C. The lysate was centrifuged at 3000 × g for 30 min and 4°C, and the pellet was resuspended in 60 mL lysis buffer (50 mM tris buffer, pH 8, 0.5 mM EDTA, 10 µg/mL aprotinin, 1 mM PMSF). Sonication was performed in 7 cycles at 60% cycle duty, power 8 for 30 sec and the homogenate was centrifuged at 73 000 × g for 45 min at 4°C. The supernatant was supplemented with 1 mM PMSF and purified first by a 2′,5′ADP Sepharose 4B column (GE Healthcare Life Sciences) then a DEAE Sepharose Fast Flow column (GE Healthcare Life Science). The concentration of holo-CPR was determined by measuring its flavin content using an extinction coefficient of 21.2 mM^{-1} cm^{-1} at 455 nm, and the activity was measured by following the reduction of cytochrome c [38].

STM bioconjugation

Mutant C215 was covalently labeled with steroid-maleimide (STM) following our published protocol, except for the removal of excess STM and reducing agents, which was achieved using centrifugal filters instead of desalting columns [34]. The mutant (1 µM, 0.7 nmol) was incubated with TCEP (45 µM, 31.5 nmol, from a 10 mM stock in 0.1 M potassium phosphate buffer, pH 7.4) at room temperature for 20 min on an orbital shaker (50 RPM). The reaction was initiated with the addition of STM (100 µM, 70 nmol from a 20 mM stock solution in anhydrous DMSO) and allowed to proceed at 4°C, for 2 h with orbital shaking (50 RPM). The reaction was quenched with DTT (2 mM, 1.4 µmol from a 100 mM stock in 0.1 M potassium phosphate buffer, pH 7.4) for 10 min at 4°C. The excess DTT, TCEP and STM were removed by buffer exchange at 4°C using Amicon Ultra-4 Centrifugal Filters (50K cutoff, 3 × 5000 RPM, 30 min, Milllipore). Control reactions (to generate the unlabeled enzyme) were treated in the same manner but with the addition of pure DMSO instead of STM. No remaining STM or DTT-quenched STM was observed by HPLC-MS after the buffer exchange (see Figures 2 and 3).
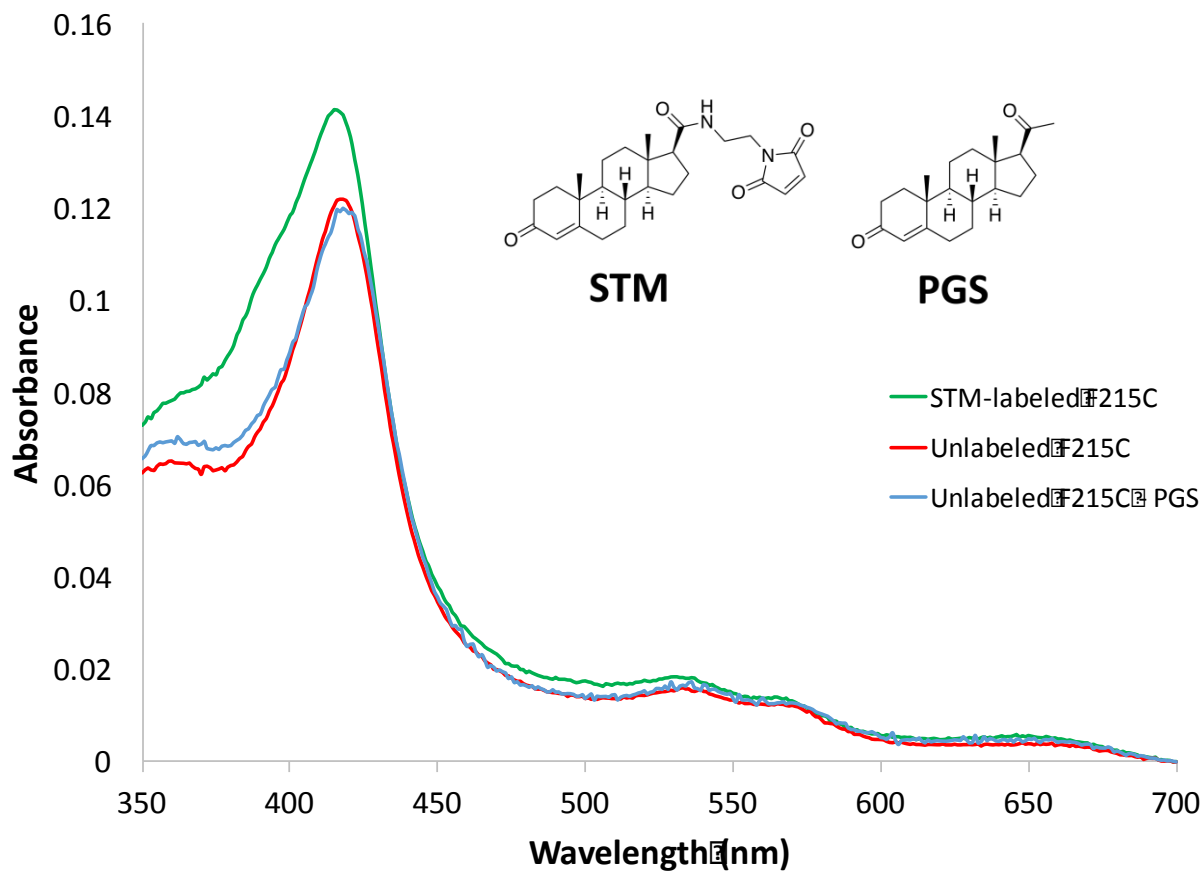
Figure 2. Absorbance spectra of the ligand-free unlabeled, STM-labeled, and PGS-treated F215C mutant of CYP3A4. To demonstrate that unconjugated STM was likely removed during the washing step and is not responsible for the high-spin shift (390 nm peak), a mock-bioconjugation control experiment was performed by treating the F215C mutant with non-modified progesterone (PGS, a good mimic of STM) under similar conditions. As evident from the absorbance spectra, the PGS-treated CYP3A4 spectrally resembles the untreated P450. Thus, the high spin shift in STM-labeled CYP3A4 is induced by the attached steroid rather than the trace amounts of non-conjugated STM that might be present in the sample.
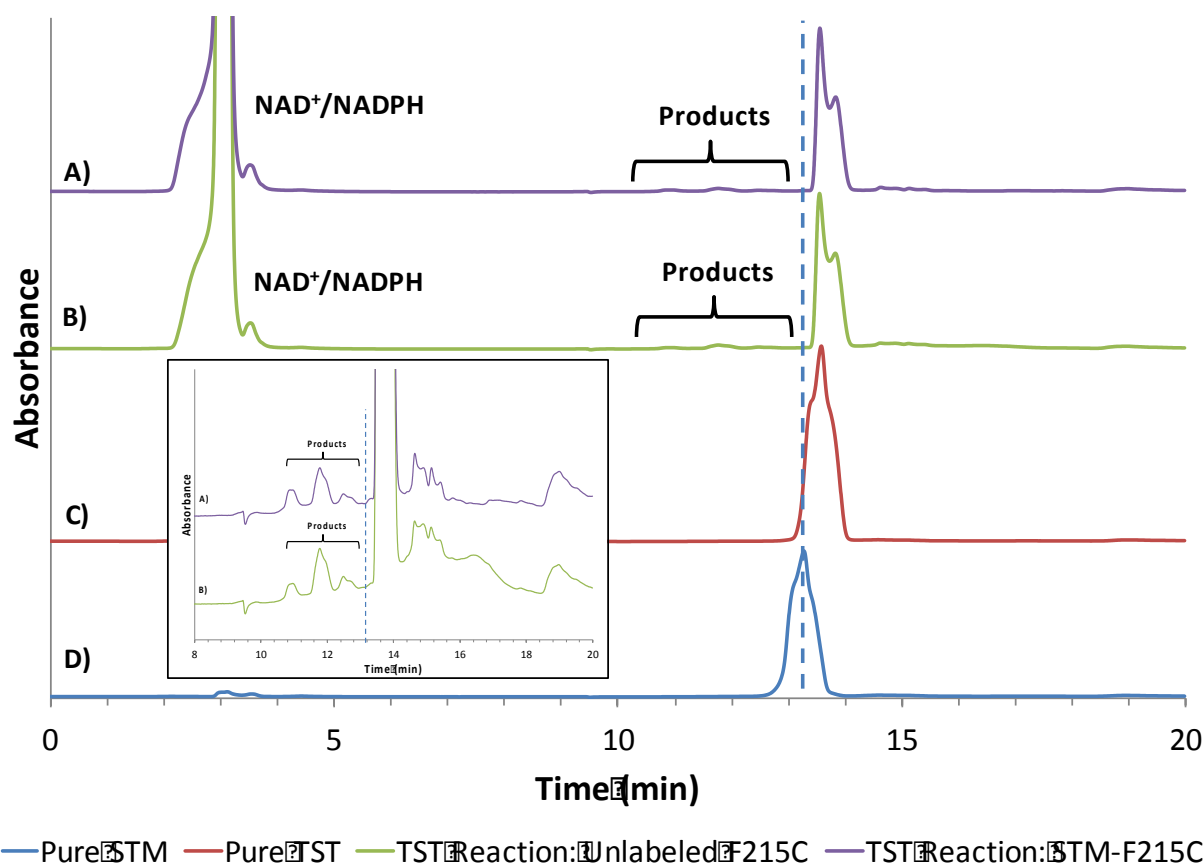
Figure 3. HPLC-UV chromatograms of the testosterone (TST) oxidation reaction by STM-labeled or unlabeled mutant F215C. A) Oxidation of TST by STM-labeled mutant F215C consisting of P450, CPR, SOD, excess TST and excess NADPH. The location of the 4 products is shown by the bracket. B) Oxidation of TST by unlabeled mutant F215C consisting of P450, CPR, SOD, excess TST and excess NADPH. The location of the products is shown by the bracket. C) Pure TST with a retention time of 13.4 min. D) Pure STM with a retention time of 13.1 min. The dashed blue line is drawn to demonstrate the expected location of STM in chromatograms A and B. The *inset* is zoomed in to show the product peaks in samples A and B.

Bioconjugation yields were calculated using an LC system coupled to a MS-QToF. Following bioconjugation, the sample was washed with Milli-Q water (3×0.5 mL) using a Spin-X UF concentrator (30K MWCO, Corning) for 15 min at $15000 \times g$. The full-length protein was analyzed by LC-MS using a Dionex Ultimate 3000 HPLC system coupled to a Bruker Maxis Impact QToF MS in positive ESI mode. Samples were run through a Poros R2/10 column from Applied Biosystems (10 μm, 2000 Å, 2.1 × 100 mm) using a gradient of 90% mobile phase A (0.1% formic acid in Milli-Q water) and 10% mobile phase B (0.1% formic acid in acetonitrile) to 0% mobile phase A and 100% mobile phase B in 15 min. The data was processed and deconvoluted using the Bruker Data Analysis software version 4.1.

The high spin content in STM-bioconjugated CYP3A4 was estimated based on the absorbance spectra of the ligand-free (100% low-spin) and bromoergocriptin-bound protein (100% high-spin conversion) samples.

Equilibrium Binding Studies

All UV-Vis spectra of the enzyme-ligand complexes were obtained on a Cary 300 UV-Vis spectrophotometer (Santa Clara, CA, USA). CYP3A4 (1 µM, 600 pmol) was dissolved in filtered PBS (593 µL, 0.6 M pH 7.5, 1 mM DTT, 20% glycerol) and added to the sample cuvette while only buffer was added to the reference cuvette. An absorbance measurement (the blank) was recorded from 350-700 nm before TST was titrated from one of two stocks (5 mM and 10 mM in DMSO) such that the total DMSO concentration never exceeded 7% (v/v), and absorbance was monitored as the TST concentration was increased. The DMSO concentrations reached had no detectable effect on the enzyme absorption spectrum. If precipitation was observed, the samples were spun down (14 000 × g) for 5 min at room temperature before acquiring the spectra. Difference spectra were plotted by subtracting the initial spectrum without TST from the consecutive spectra with TST. The difference in the absorbance between 405 nm and 418 nm (trough) was plotted against substrate concentration to obtain a binding curve. Spectral dissociation constants (K_S) were derived from the binding curves using the GraphPad software. The data were fit to Equation 1, where ΔA is the difference in absorbance between the peak and trough, ΔA_{max} is the maximum reachable value for ΔA at saturating substrate concentration, [S] is the substrate concentration, K_S is the substrate concentration at half saturation and n is the Hill coefficient, which is indicative of the cooperativity of a system.

Equation 1:
$$\Delta A = \frac{\Delta A_{max} \times [S]^n}{K_S^n + [S]^n}$$

Coupling of TST oxidation to NADPH consumption

CYP3A4 (5 µM, 1 nmol), CPR (5 µM, 1 nmol) and superoxide dismutase (2.5 µM, 0.5 nmol) were combined in potassium phosphate buffer (0.1 M, pH 7.4), with or without TST (100 µM, 20 nmol, 10 mM stock in DMSO) and incubated at room temperature for 30 min. The reaction was initiated with NADPH (1 mM, 200 nmol, stock in Milli-Q water) and NADPH consumption was monitored by UV-Vis at room temperature until completion. The reaction was diluted in acetonitrile (100 µL), vortexed for 1 min and centrifuged at 21 000 × g for 5 min. The supernatant was diluted in buffer (100 µL) and directly analyzed by HPLC-UV-MS. MS detection was used to identify the products and UV detection was used to quantify each product based on a calibration curve. The separation and quantification of the products was achieved using an Eclipse XDB-C18 (5 µm, 4.6 × 150 mm) column in line with a UV detector (set to monitor at 244 nm) and mobile phases A (Milli-Q water) and B (acetonitrile) at a flow rate of 0.5 mL/min. The elution entailed an isocratic step at 100% phase A for 3 min, followed by an increase to 95% phase B over 12 min before an isocratic step at 95% phase B over 5 min. The retention times were: 13.9 min for the major product 6β-hydroxy-TST, 13.5 min, 14.4 min and 15.0 min for the minor hydroxylated TST products (likely 1β-hydroxy-TST, 2β-hydroxy-TST, 15β-hydroxy-TST as suggested by Krauser [39]), and 16.5 min for TST. The product yield was calculated by converting the sum of the areas under the UV peaks of all products into a concentration (µM) using a calibration curve and TST as the standard. The coupling efficiency was determined using Equation 2.

Equation 2: $\text{Coupling efficiency (\%)} = \dfrac{\text{[Total amount of hydroxytestosterone products] μM}}{\text{[Total amount of NADPH consumed] μM}} \times 100$

Coupling of BFC oxidation to NADPH consumption

To determine the initial rate of NADPH consumption, CYP3A4 (1 µM, 0.2 nmol), CPR (1 µM, 0.2 nmol) and superoxide dismutase (2.5 µM, 0.5 nmol) were combined in PBS (0.1 M, pH 7.4), with or without BFC (100 µM, 20 nmol, 10 mM stock in DMSO) and incubated at room temperature for 30 min. The reaction was initiated with the addition of NADPH (200 µM, 40 nmol, stock in Milli-Q water) and NADPH consumption was monitored at 340 nm and room temperature for 8 min, with the data remaining linear throughout the measurements. The initial rate of NADPH consumption was determined from the change in absorbance over 3 min and converted to concentration (µM) using an extinction coefficient of 6220 $M^{-1}cm^{-1}$. The concentration of BFC used was selected to be saturating based on the reported K_M, which ranges from 26 – 48 µM [34,40,41].

Formation of the fluorescent product, 7-hydroxy-4-trifluoromethyl coumarin (HFC) was assayed under the same experimental conditions using a microtiter plate fluorimeter (SpectraMax i3, Molecular Device). The initial rate of HFC production was determined from the change in fluorescence over 15 min, with the data remaining linear throughout the measurements, and converted to concentration (µM) using a calibration curve. The coupling efficiency was calculated using Equation 3.

Equation 3: $\text{Coupling efficiency (\%)} = \dfrac{\text{[Rate of HFC production] μM/min}}{\text{[Rate of NADPH consumption] μM/min}} \times 100$

Results and Discussion

To further study the effect of steroids on the ligand binding and functional activity of CYP3A4, a steroid analogue (STM) containing a maleimide functional group was regioselectively bioconjugated to a CYP3A4 mutant, as previously described [34]. Based on structural similarity between STM and the steroids progesterone and TST (Figure 1), we reason that it could be a good mimic of both molecules. A cysteine depleted mutant (C58T/C64A/C98S/C239S/C468G) with a newly introduced cysteine (F215C) was used to achieve site-selective bioconjugation in high yield (> 84% as estimated by HPLC-MS-QToF). The STM-labeled and unlabeled preparations of CYP3A4 used in this study were treated under similar bioconjugation conditions, except for the lack of STM in the unlabeled sample.

Spectral differences between the unlabeled and STM-labeled CYP3A4

In the resting state, cytochrome P450 enzymes have a Soret absorption peak at 416-418 nm, corresponding to the hexa-coordinated heme iron (low-spin state) with water as the 6th ligand. Upon substrate binding, the water molecule uncoordinates from the iron, resulting in a penta-coordinated heme iron (high-spin state) which absorbs light at 380-390 nm. Absorbance spectra of both STM-labeled and unlabeled CYP3A4 have their Soret peak at 418 nm (Figure 4). However, a unique feature of STM-labeled enzyme is a pronounced shoulder at 386 nm due to a larger content of the high-spin state heme (~15%). A low-to-high spin shift usually takes place

upon substrate (type I ligand) binding, with the high-spin content depending on the nature of the ligand. To ensure that the high-spin shift is not caused by the residual amounts of non-conjugated STM, a mock-bioconjugation control experiment was performed, where the F215C mutant was treated with PGS under the same conditions. As shown in Figure 2, there were no visible spectral changes in the PGS-treated CYP3A4.

Without crystallographic evidence, it is difficult to rationalize the structural effect of the covalently-linked progesterone molecule on the spin state of CYP3A4. The high-spin shift may be due to partial reorientation of the linked steroid from the allosteric site into the active site and displacement of the distal water ligand, or due to an allosteric effect on the enzyme structure. Previous reports were not able to detect changes in the spin state for the first progesterone binding event [18,19,42]. However, studies on the CYP3A4-TST interaction have suggested that even the first binding event notably increases the amount of high-spin species (to 25%) [17,19], consistent with what is observed here. Association of the first TST molecule at the allosteric site and the resulting high-spin shift may explain why there is no product formation for the one-bound species despite the increased NADPH oxidation rate [17,19].
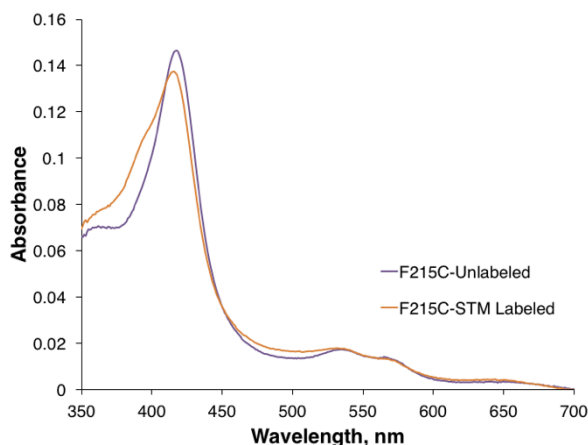

Figure 4. Absorbance spectra of the purified STM-labeled and unlabeled CYP3A4 C215 mutant. Both enzymes are predominantly in the low-spin state (418 nm peak), but the STM-labeled mutant has the larger high-spin content (a pronounced shoulder at 386 nm). The high spin content in STM-bioconjugated CYP3A4 (~15%) was estimated based on the absorbance spectra of the ligand-free (100% low-spin) and bromoergocriptin-bound protein (100% high-spin conversion) samples.

Equilibrium binding titrations

To investigate whether STM bioconjugation at the allosteric site affects ligand binding, the affinity of both the STM-labeled and unlabeled CYP3A4 for TST was determined *via* equilibrium binding titrations. Spectral changes were monitored in the 405-420 nm region, regularly used for studying substrate binding to CYPs and for determination of the spectral binding constant (K_S), a measure of the ligand binding affinity [13,43–48]. A clear difference was observed in the binding affinity of TST for the labeled and unlabeled CYP3A4 (Figure 5). The K_S for the STM-labeled enzyme was ~1.4 × higher than that for the unlabeled species (158

vs 110 µM, respectively), suggesting that attachment of a steroid at the allosteric site reduces the affinity of the enzyme for TST. This is in line with the hypothesis that the peripheral area is a high affinity site that is occupied first, followed by association of the subsequent TST molecules to the lower affinity sites located within the active site pocket [17,19,28]. Since in the labeled CYP3A4 the high affinity site is already occupied, the measured K_S value reflects the binding event to the lower affinity sites. In other words, the STM attachment to the allosteric site simplifies the system by decreasing the number of binding events from three to two.

While the Hill coefficient (*n*) calculated for the unlabeled enzyme (1.10 ± 0.09) suggests minimal positive cooperativity for TST binding to CYP3A4, no cooperativity is observed for the STM-labeled species (0.97 ± 0.05). Both results, however, are within error and their differences could also be considered negligible. Due to poor solubility and the negligible spectral changes induced by BFC, its K_S for the enzymes could not be determined.
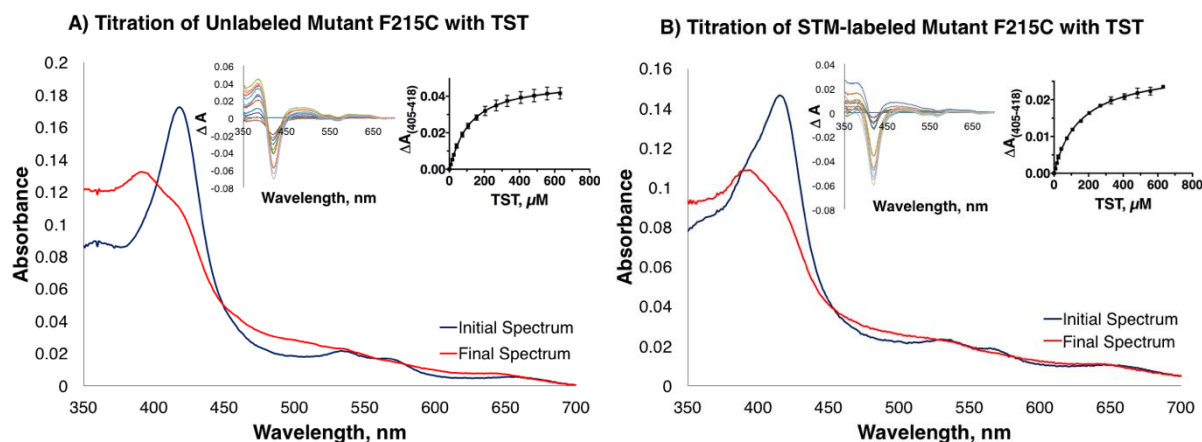
	Unlabeled	STM Labeled
K_S (µM)	110 ± 13	158 ± 16
n	1.10 ± 0.09	0.97 ± 0.05

Figure 5. Titrations of STM-labeled and unlabeled mutant CYP3A4 with TST.
Only the initial and final absorbance spectra recorded during equilibrium titrations of the unlabeled (A) and STM-labeled enzyme (B) with TST are displayed. *Insets* show the difference spectra for the entire titration (left panels) and the derived titration plots with fitting curves (right panels). The spectral binding constants (K_S) and Hill coefficient (*n*) are listed in the adjacent table as an average of three replicates with the standard error.

NADPH Consumption

We next looked at the effect of steroid bioconjugation on the rate of NADPH consumption. Table 1 shows the rates of NADPH consumption for both STM-labeled and unlabeled CYP3A4 in the presence and absence of substrate. In the absence of substrate, the STM-labeled CYP3A4 consumed $1.4 \times$ more NADPH (4.5 ± 0.2 µmol/min/µmol) than the unlabeled enzyme (3.2 ± 0.5 µmol/min/µmol). This may be the result of the larger high-spin content in STM-labeled CYP3A4 (Figure 4), known to promote the inter-protein electron

transfer. At saturating TST concentrations, when all binding sites are occupied and the heme iron is almost fully in the high-spin state (Figure 5), the NADPH oxidation rates for the unlabeled and labeled CYP3A4 were similar: 5.0 and 4.4 µmol/min/µmol, respectively. This is consistent with both enzyme species being saturated with ligand. In the presence of a saturating concentration of BFC, the NADPH consumption rates were also similar (2.0 and 2.3 µmol/min/µmol for the labeled and unlabeled enzyme, respectively) and 2-fold lower than the respective rates measured in the absence of substrate (Table 1). It is unclear at the moment how BFC exerts this negative effect. In any case, the rate of NADPH oxidation by the unlabeled mutant was comparable to that for the wild type enzyme (3.5, 2.0 and 3.6 µmol/min/µmol for no substrate, BFC and TST, respectively) and, therefore, the CYP3A4 mutant could serve as a model for the wild type enzyme.

Table 1. Coupling parameters for BFC and TST for unlabeled and STM-labeled mutant CYP3A4[a]

CYP3A4 Variant	Substrate	NADPH consumption[b]	HFC produced[b]	TST-OH produced[c]	Coupling %[d]
Unlabeled CYP3A4	none	3.2 ± 0.5	n.a.[e]	n.a.	n.a.
	+ BFC	2.0 ± 0.7	0.0044 ± 0.0008	n.a.	0.2 ± 0.1
	+ TST	5.0 ± 0.1	n.a.	8.6 ± 0.7	0.9 ± 0.1
STM-labeled CYP3A4	none	4.5 ± 0.2	n.a.	n.a.	n.a.
	+ BFC	2.3 ± 0.6	0.012 ± 0.002	n.a.	0.5 ± 0.1
	+ TST	4.4 ± 0.1	n.a.	9.0 ± 1.9	0.9 ± 0.2

[a]Each result is an average of two experiments performed in duplicates, with the standard deviation shown.
[b]Reported in µmol/min/µmol enzyme.
[c]The amount of all hydroxytestosterone products (TST-OH; in µM) formed upon consumption of 1000 µM NADPH.
[d]With the substrate BFC, the coupling efficiency is determined by comparing the rate of HFC production to that of NADPH consumption. With the substrate TST, the coupling efficiency is determined by comparing the total amount of TST-OH produced (in µM) to the total amount of NADPH consumed (1000 µM).
[e]n.a.: data point is not applicable because it is not related to the substrate of interest.

Coupling efficiency

CYP3A4 is well known for being a poorly coupled enzyme, meaning that a large portion of the reducing equivalents from NADPH are used to generate by-products (hydrogen peroxide, superoxide and/or water) rather than the oxidized substrate [17–20,42,49,50]. Thus, the effectiveness of CYP3A4 catalysis can be quantified in terms of coupling efficiency, which relates the amount of oxidized product formed to the amount of NADPH consumed. The effect of STM bioconjugation at the allosteric site on the coupling efficiency of CYP3A4 was next investigated for both BFC and TST (Table 1).

BFC is oxidized by CYP3A4 to produce the fluorescent product HFC. The production of HFC was monitored to determine the initial rate of BFC oxidation, which was compared to the

initial rate of NADPH consumption to determine the coupling efficiency. It was observed that the STM-labeled mutant metabolizes BFC 2.7 × faster than the unlabeled control, yet the rate of NADPH consumption was similar for both (Table 1). This suggests that the STM-labeled enzyme is better coupled than the unlabeled control (0.5% vs 0.2%, respectively), and that the enhanced coupling is due to a more effective BFC transformation rather than changes in the NADPH consumption rate.

The coupling efficiency with the substrate TST was determined by an end-point assay which compares the total amount of hydroxytestosterone produced (TST-OH, total of all regioisomers produced) and the amount of NADPH consumed (1000 µM). HPLC-UV chromatograms for TST oxidation by the STM-labeled and unlabeled F215C mutant are shown in Figure 3. It should be noted that neither the mutagenesis, nor the bioconjugation were found to modify the product profile of this enzymatic reaction. The results show similar coupling efficiency for both the STM-labeled and unlabeled species (~0.9%). Moreover, the coupling efficiency of the unlabeled enzyme was comparable to that of the wild type enzyme (0.3% and 1% for BFC and TST, respectively), once again suggesting that the behaviour of the mutant may be representative of that of the wild type enzyme.

In summary, we have demonstrated how bioconjugation can be used to simplify studies of enzymes capable of binding multiple ligands simultaneously. By conjugating a steroid to a postulated allosteric site in CYP3A4, we were able to determine its effect on the ligand binding affinity and enzyme coupling efficiency. Our results are consistent with the hypothesis that an allosteric pocket is the higher affinity binding site of TST, and reveal an increased coupling efficiency of the STM-labeled CYP3A4 (at least for BFC) due to an increased rate of substrate oxidation. Moreover, for the first time, we provide direct evidence for the formation of high-spin species upon bioconjugation at the allosteric site, which has been anticipated but only indirectly modelled before [18,19,42].

Disclosure Statement
The authors declare no competing financial interest

References

[1]   F.P. Guengerich, Human Cytochrome P450 Enzymes, in: P.R. Ortiz de Montellano (Ed.), Cytochrome P450, 3rd ed., Springer US, Boston, MA, 2015: pp. 377–530. doi:10.1007/0-387-27447-2_10.

[2]   F.P. Guengerich, Cytochrome P-450 3A4: regulation and role in drug metabolism, Annu. Rev. Pharmacol. Toxicol. 39 (1999) 1–17. doi:10.1146/annurev.pharmtox.39.1.1.

[3]   I.G. Denisov, D.J. Frank, S.G. Sligar, Cooperative properties of cytochromes P450, Pharmacol. Ther. 124 (2009) 151–167. doi:10.1016/j.pharmthera.2009.05.011.

[4]   M. Ekroos, T. Sjögren, Structural basis for ligand promiscuity in cytochrome P450 3A4, Proc. Natl. Acad. Sci. U. S. A. 103 (2006) 13682–13687. doi:10.1073/pnas.0603236103.

[5]   P.A. Williams, J. Cosme, D. Matak Vinković, A. Ward, H.C. Angove, P.J. Day, C. Vonrhein, I.J. Tickle, H. Jhoti, Crystal structures of human cytochrome P450 3A4 bound to metyrapone and progesterone, Science (80-.). 305 (2004) 683–686. doi:10.1126/science.1099736.

[6]   I.F. Sevrioukova, High-Level Production and Properties of the Cysteine-Depleted Cytochrome P450 3A4, Biochemistry. 56 (2017) 3058–3067. doi:10.1021/acs.biochem.7b00334.

[7]   J.K. Yano, M.R. Wester, G.A. Schoch, K.J. Griffin, C.D. Stout, E.F. Johnson, The structure of human microsomal cytochrome P450 3A4 determined by X-ray crystallography to 2.05-A resolution, J. Biol. Chem. 279 (2004) 38091–38094. doi:10.1074/jbc.C400293200.

[8]   G. Brändén, T. Sjögren, V. Schnecke, Y. Xue, Structure-based ligand design to overcome CYP inhibition in drug discovery projects, Drug Discov. Today. 19 (2014) 905–911. doi:10.1016/j.drudis.2014.03.012.

[9]   I.F. Sevrioukova, T.L. Poulos, Structural basis for regiospecific midazolam oxidation by human cytochrome P450 3A4, Proc. Natl. Acad. Sci. 114 (2017) 486–491. doi:10.1073/pnas.1616198114.

[10]   I.F. Sevrioukova, T.L. Poulos, Structural and mechanistic insights into the interaction of cytochrome P4503A4 with bromoergocryptine, a type I ligand, J. Biol. Chem. 287 (2012) 3510–3517. doi:10.1074/jbc.M111.317081.

[11]   I.F. Sevrioukova, T.L. Poulos, Structure and mechanism of the complex between cytochrome P4503A4 and ritonavir, Proc. Natl. Acad. Sci. U. S. A. 107 (2010) 18422–18427. doi:10.1073/pnas.1010693107.

[12]   P. Kaur, A.R. Chamberlin, T.L. Poulos, I.F. Sevrioukova, Structure-Based Inhibitor Design for Evaluation of a CYP3A4 Pharmacophore Model, J. Med. Chem. 59 (2016) 4210–4220. doi:10.1021/acs.jmedchem.5b01146.

[13]   T.L. Poulos, I.F. Sevrioukova, Current Approaches for Investigating and Predicting Cytochrome P450 3A4-Ligand Interactions, Springer International Publishing, Cham, 2015. doi:10.1007/978-3-319-16009-2.

[14]   Z. Guo, I.F. Sevrioukova, I.G. Denisov, X. Zhang, T.L. Chiu, D.G. Thomas, E.A. Hanse, R.A.D. Cuellar, Y. V Grinkova, V.W. Langenfeld, D.S. Swedien, J.D. Stamschror, J. Alvarez, F. Luna, A. Galván, Y.K. Bae, J.D. Wulfkuhle, R.I. Gallagher, E.F. Petricoin, B. Norris, C.M. Flory, R.J. Schumacher, M.G. O'Sullivan, Q. Cao, H. Chu, J.D. Lipscomb, W.M. Atkins, K. Gupta, A. Kelekar, I.A. Blair, J.H. Capdevila, J.R. Falck, S.G. Sligar, T.L. Poulos, G.I. Georg, E. Ambrose, D.A. Potter, Heme Binding Biguanides Target Cytochrome P450-Dependent Cancer Cell Mitochondria, Cell Chem. Biol. 24 (2017)

1259–1275.e6. doi:10.1016/j.chembiol.2017.08.009.

[15] W.K. Childers, J.P. Harrelson, Allosteric modulation of substrate motion in cytochrome P450 3A4-mediated xylene oxidation, Biochemistry. 53 (2014) 1018–1028. doi:10.1021/bi401472p.

[16] P.A. Kelly, H. Wang, K.L. Napoli, B.D. Kahan, H.W. Strobel, Metabolism of cyclosporine by cytochromes P450 3A9 and 3A4, Eur. J. Drug Metab. Pharmacokinet. 24 (1999) 321–328. doi:10.1007/BF03190040.

[17] I.G. Denisov, B.J. Baas, Y. V Grinkova, S.G. Sligar, Cooperativity in cytochrome P450 3A4: linkages in substrate binding, spin state, uncoupling, and product formation, J. Biol. Chem. 282 (2007) 7066–7076. doi:10.1074/jbc.M609589200.

[18] I.G. Denisov, Y. V Grinkova, J.L. Baylon, E. Tajkhorshid, S.G. Sligar, Mechanism of Drug–Drug Interactions Mediated by Human Cytochrome P450 CYP3A4 Monomer, Biochemistry. 54 (2015) 2227–2239. doi:10.1021/acs.biochem.5b00079.

[19] D.J. Frank, I.G. Denisov, S.G. Sligar, Analysis of heterotropic cooperativity in cytochrome P450 3A4 using alpha-naphthoflavone and testosterone, J. Biol. Chem. 286 (2011) 5540–5545. doi:10.1074/jbc.M110.182055.

[20] Y.-F. Ueng, T. Kuwabara, Y.-J. Chun, F.P. Guengerich, Cooperativity in oxidations catalyzed by cytochrome P450 3A4, Biochemistry. 36 (1997) 370–381. doi:10.1021/bi962359z.

[21] M. Shou, Q. Mei, M.W. Ettore, Jr., R. Dai, T.A. Baillie, T.H. Rushmore, Sigmoidal kinetic model for two co-operative substrate-binding sites in a cytochrome P450 3A4 active site: an example of the metabolism of diazepam and its derivatives, Biochem. J. 340 (1999) 845–853. doi:10.1042/0264-6021:3400845.

[22] J.M. Hutzler, T.S. Tracy, Atypical kinetic profiles in drug metabolism reactions, Drug Metab. Dispos. 30 (2002) 355–362. doi:10.1124/dmd.30.4.355.

[23] D.R. Davydov, Z. Yang, N. Davydova, J.R. Halpert, W.L. Hubbell, Conformational Mobility in Cytochrome P450 3A4 Explored by Pressure-Perturbation EPR Spectroscopy, Biophys. J. 110 (2016) 1485–1498. doi:10.1016/j.bpj.2016.02.026.

[24] K.K. Khan, Y.Q. He, T.L. Domanski, J.R. Halpert, Midazolam Oxidation by Cytochrome P450 3A4 and Active-Site Mutants: an Evaluation of Multiple Binding Sites and of the Metabolic Pathway That Leads to Enzyme Inactivation, Mol. Pharmacol. 61 (2002) 495–506.

[25] I.F. Sevrioukova, T.L. Poulos, Anion-Dependent Stimulation of CYP3A4 Monooxygenase, Biochemistry. 54 (2015) 4083–4096. doi:10.1021/acs.biochem.5b00510.

[26] T.L. Domanski, Y.-A. He, K.K. Khan, F. Roussel, Q. Wang, J.R. Halpert, Phenylalanine and Tryptophan Scanning Mutagenesis of CYP3A4 Substrate Recognition Site Residues and Effect on Substrate Oxidation and Cooperativity, Biochemistry. 40 (2001) 10150–10160. doi:10.1021/bi010758a.

[27] G.R. Harlow, J.R. Halpert, Alanine-scanning Mutagenesis of a Putative Substrate Recognition Site in Human Cytochrome P450 3A4, J. Biol. Chem. 272 (1997) 5396–5402. doi:10.1074/jbc.272.9.5396.

[28] D.J. Frank, I.G. Denisov, S.G. Sligar, Mixing apples and oranges: Analysis of heterotropic cooperativity in cytochrome P450 3A4, Arch. Biochem. Biophys. 488 (2009) 146–152. doi:10.1016/j.abb.2009.06.013.

[29] D.R. Davydov, J.A.O. Rumfeldt, E. V Sineva, H. Fernando, N.Y. Davydova, J.R. Halpert, Peripheral ligand-binding site in cytochrome P450 3A4 located with fluorescence

resonance energy transfer (FRET), J. Biol. Chem. 287 (2012) 6797–809. doi:10.1074/jbc.M111.325654.

[30] G.R. Harlow, J.R. Halpert, Analysis of human cytochrome P450 3A4 cooperativity: construction and characterization of a site-directed mutant that displays hyperbolic steroid hydroxylation kinetics., Proc. Natl. Acad. Sci. U. S. A. 95 (1998) 6636–6641. http://www.pubmedcentral.nih.gov/articlerender.fcgi?artid=22578&tool=pmcentrez&rendertype=abstract.

[31] G.A. Marsch, B.T. Carlson, F.P. Guengerich, 7,8-benzoflavone binding to human cytochrome P450 3A4 reveals complex fluorescence quenching, suggesting binding at multiple protein sites, J. Biomol. Struct. Dyn. (2017) 1–20. doi:10.1080/07391102.2017.1301270.

[32] C.M. Woods, C. Fernandez, K.L. Kunze, W.M. Atkins, Allosteric activation of cytochrome P450 3A4 by α-naphthoflavone: Branch point regulation revealed by isotope dilution analysis, Biochemistry. 50 (2011) 10041–10051. doi:10.1021/bi2013454.

[33] A.G. Roberts, A.P. Campbell, W.M. Atkins, The Thermodynamic Landscape of Testosterone Binding to Cytochrome P450 3A4: Ligand Binding and Spin State Equilibria, Biochemistry. 44 (2005) 1353–1366. doi:10.1021/bi0481390.

[34] V. Polic, K. Auclair, Allosteric Activation of Cytochrome P450 3A4 via Progesterone Bioconjugation, Bioconjug. Chem. 28 (2017) 885–889. doi:10.1021/acs.bioconjchem.6b00604.

[35] E.F. Pettersen, T.D. Goddard, C.C. Huang, G.S. Couch, D.M. Greenblatt, E.C. Meng, T.E. Ferrin, UCSF Chimera - A visualization system for exploratory research and analysis, J. Comput. Chem. 25 (2004) 1605–1612. doi:10.1002/jcc.20084.

[36] A. Menard, Y. Huang, P. Karam, G. Cosa, K. Auclair, Site-Specific Fluorescent Labeling and Oriented Immobilization of a Triple Mutant of CYP3A4 via C64, Bioconjug. Chem. 23 (2012) 826–836. doi:10.1021/bc200672s.

[37] T. Omura, R. Sato, The Carbon Monoxide-binding Pigment of Liver Microsomes: 2. Solubilization, Purification and Properties, J. Biol. Chem. 239 (1964) 2379–2385. http://www.jbc.org/content/239/7/2379.short.

[38] A. Chefson, J. Zhao, K. Auclair, Replacement of Natural Cofactors by Selected Hydrogen Peroxide Donors or Organic Peroxides Results in Improved Activity for CYP3A4 and CYP2D6, ChemBioChem. 7 (2006) 916–919. doi:10.1002/cbic.200600006.

[39] J.A. Krauser, M. Voehler, L.-H. Tseng, A.B. Schefer, M. Godejohann, F.P. Guengerich, Testosterone 1 beta-hydroxylation by human cytochrome P450 3A4., Eur. J. Biochem. 271 (2004) 3962–9. doi:10.1111/j.1432-1033.2004.04339.x.

[40] M.T. Donato, N. Jimenez, J. V. Castell, M.J. Gomez-Lechon, Fluorescence-Based Assays For Screening Nine Cytochrome P450 (P450) Activities in Intact Cells Expressing Individual Human P450 Enzymes, Drug Metab. Dispos. 32 (2004) 699–706.

[41] P. Lu, Y.U.H. Lin, A.D. Rodrigues, T.H. Rushmore, T.A. Baillie, M. Shou, Testosterone, 7-Benzyloxyquinoline, and 7-benzyloxy-4-trifluoromethyl-coumarin bind to different domains within the active site of cytochrome P450 3A4, Drug Metab. Dispos. 29 (2001) 1473–1479.

[42] I.G. Denisov, J.L. Baylon, Y. V Grinkova, E. Tajkhorshid, S.G. Sligar, Drug–Drug Interactions between Atorvastatin and Dronedarone Mediated by Monomeric CYP3A4, Biochemistry. 57 (2018) 805–816. doi:10.1021/acs.biochem.7b01012.

[43] D.R. Davydov, N.Y. Davydova, T.N. Tsalkova, J.R. Halpert, Effect of glutathione on

homo- and heterotropic cooperativity in cytochrome P450 3A4, Arch. Biochem. Biophys. 471 (2008) 134–145. doi:10.1016/j.abb.2008.01.001.

[44] T. Ichikawa, H. Tsujino, T. Miki, M. Kobayashi, C. Matsubara, S. Miyata, T. Yamashita, K. Takeshita, Y. Yonezawa, T. Uno, Allosteric activation of cytochrome P450 3A4 by efavirenz facilitates midazolam binding, Xenobiotica. (2017) 1–10. doi:10.1080/00498254.2017.1412540.

[45] K.W. Anderson, N. Mast, J.W. Hudgens, J.B. Lin, I. V Turko, I.A. Pikuleva, Mapping of the allosteric site in cholesterol hydroxylase CYP46A1 for efavirenz, a drug that stimulates enzyme activity, J. Biol. Chem. 291 (2016) 11876–11886. doi:10.1074/jbc.M116.723577.

[46] S.G. Sligar, Coupling of spin, substrate, and redox equilibriums in cytochrome P450, Biochemistry. 15 (1976) 5399–5406. doi:10.1021/bi00669a029.

[47] E.M. Isin, F.P. Guengerich, Kinetics and thermodynamics of ligand binding by cytochrome P450 3A4, J. Biol. Chem. 281 (2006) 9127–9136. doi:10.1074/jbc.M511375200.

[48] I.G. Denisov, P.J. Mak, Y. V Grinkova, D. Bastien, G. Bérubé, S.G. Sligar, J.R. Kincaid, The use of isomeric testosterone dimers to explore allosteric effects in substrate binding to cytochrome P450 CYP3A4, J. Inorg. Biochem. 158 (2016) 77–85. doi:10.1016/j.jinorgbio.2015.12.019.

[49] Y. V Grinkova, I.G. Denisov, M.A. McLean, S.G. Sligar, Oxidase uncoupling in heme monooxygenases: Human cytochrome P450 CYP3A4 in Nanodiscs, Biochem. Biophys. Res. Commun. 430 (2013) 1223–1227. doi:10.1016/j.bbrc.2012.12.072.

[50] A. Perret, D. Pompon, Electron shuttle between membrane-bound cytochrome P450 3A4 and b5 rules uncoupling mechanisms, Biochemistry. 37 (1998) 11412–11424. doi:10.1021/bi980908q.